DEUTSCHES ELEKTRONEN-SYNCHROTRON DESY

DESY 80/38
May 1980

EXPERIENCE WITH THE JADE JET-CHAMBER AT PETRA

AND

PATTERN RECOGNITION PROGRAMS FOR THE JADE JET-CHAMBER

by

H. Drumm, B. Granz, J. Heintze, G. Heinzelmann,
R. D. Heuer, J. van Krogh, P. Lennert, T. Nozaki,
H. Rieseberg, A. Wagner
Physikalisches Institut der Universität Heidelberg

R. Eichler, J. Olsson, P. Steffen
Deutsches Elektronen-Synchrotron DESY, Hamburg

M. C. Goddard, G. F. Pearce
Rutherford Laboratory, Chilton, England

P. Warming
II. Physikalisches Institut der Universität Hamburg

NOTKESTRASSE 85 · 2 HAMBURG 52

To be sure that your preprints are promptly included in the
HIGH ENERGY PHYSICS INDEX ,
send them to the following address (if possible by air mail) :

DESY
Bibliothek
Notkestrasse 85
2 Hamburg 52
Germany

DESY 80/38
May 1980

Experience with the JADE JET-Chamber at PETRA

and

Pattern Recognition Programs for the JADE JET-Chamber *

H. Drumm[1], R. Eichler[2], M.C. Goddard[3], B. Granz[1,4], J. Heintze[1], G. Heinzelmann[1], R.D. Heuer[1], J. van Krogh[1], P. Lennert[1], T. Nozaki[1], J. Olsson[2], G.F. Pearce[3], H. Rieseberg[1], P. Steffen[2], A. Wagner[1], P. Warming[5].

Contributions to the 1980 Wire Chamber Conference at Vienna
(Presented by A. Wagner and P. Steffen)

* Work supported in part by the W. German Bundesministerium für Forschung und Technologie.

1) Physikalisches Institut der Universität Heidelberg, Germany
2) Deutsches Elektronen-Synchrotron DESY, Hamburg, Germany
3) Rutherford Laboratory, Chilton, England
4) now at Siemens A.G., Erlangen
5) II. Physikalisches Institut der Universität Hamburg.

Abstracts :

This report contains the contributions to the 1980 Wire Chamber Conference at Vienna concerning the JADE JET-Chamber.

Part 1 :

The principle of the jet-chamber, a pictorial driftchamber serving as the central track detector of the JADE experiment at PETRA is briefly reviewed. In this chamber, up to 48 points are measured along each track. At each point the space coordinates R, ϕ, Z and the energy loss dE/dx of charged particles are recorded. The present status of the space resolution and of energy loss measurements is described. Experience during nine months of operation is reported.

Part 2 :

Pattern recognition programs developed for the jet chambers of the JADE experiment are described. A method is presented which allows a fast determination of the event vertex along the beam direction without prior track finding. The track finding itself starts with the complete set of measured points per track and reduces this information to line elements, track elements and tracks. The efficiency obtained so far for jet events with a high track density is 97 % per track. In addition a graphics program is described which allows interactive guidance of the pattern recognition.

Part 1 :

1. Introduction

For the central tracking chamber of the JADE detector [1] (Fig. 1) at the e^+e^- storage ring PETRA a new concept of a pictorial drift chamber, the so-called jet-chamber, has been developed.[1] The chamber has to be capable to record events of a high local track density (jets) with good space- and double track resolution and with the possibility of particle identification within a solid angle close to 4π sterad. It is operated at elevated gas pressure. This is essential for the particle identification by energy loss measurement and for an improvement of the spatial resolution.

In section 2 the most important features of the chamber are summarized. Details about the principle of the jet-chamber, its construction and the electronics have already been published[2) 5)] or are reviewed at this conference[3)]. Section 3 contains a discussion of the present status of the space resolution, the momentum resolution and the particle identification. In section 4 the performance of the chamber during the first 9 months of operation at PETRA is discussed. Since the calibration of the detector is not yet in its final form, all numbers are preliminary.

2. The principle of the jet-chamber

The sensitive volume of the driftchamber is a cylinder with a diameter of 1.6 meters and a length of 2.4 meters. The cylinder is divided into 24 segments, forming a bicycle wheel geometry. Each segment subtends an azimuthal angle of 15 degrees. Two such segments are shown in Fig. 2. Each segment forms a mechanical selfsupporting unit and is subdivided into 4 cells. Each cell contains in the median plane 16 anode wires separated by potential wires. A drift field of 940 V/cm with equipotential planes parallel to the median plane is provided by field electrodes connected to

high voltage (6 kV to 9 kV depending on the cell size). The anodes wires are kept at ground potential. The gas gain can be adjusted through the high voltage applied to the potential wires (approx. 2.4 kV).

In the range of polar angle $34^\circ < \theta < 146^\circ$ (with respect to the direction of the incident beam) 48 points are measured along each track. The first point on the track is measured at a radius of 21 cm, the last point at 79 cm. For polar angles $\theta < 34^\circ$ and $\theta > 146^\circ$ a reduced number of points is recorded. At least 8 points on a track are obtained over a solid angle of 97% of the full sphere. The high number of space points improves the reliability of pattern recognition in the case of complex events. Details concerning the pattern recognition can be found in ref. 4. Fig. 3 shows a typical jet event.

At each point the three dimensional coordinates (R, Φ, Z) are given by the wire position, the drift time and by charge division measurements. The charge division method requires the measurement of the integrated charge from each hit at both ends of the signal wire. The ratio of these amplitudes determines Z and the sum of both amplitudes measures the energy loss dE/dx of the particle in the chamber gas. Different tracks within one cell do not interfere with each other provided they are separated by drift times greater than the sum of integration- and dead time. The double track resolution can be verified by adjustment of the integration time, which is currently set to 120 ns, leading to a double track resolution of 7 mm.

The left / right ambiguity is resolved by staggering the anode wires alternatingly to the left and right hand side of the median plane. The staggering is $\pm$ 150 µm, to which 50 µm is added through electrostatic deflection. This arrangement provides a unique resolution of the ambiguity [2)].

The electronics connected to the 1536 wires of the detector is schematically shown in Fig. 4. Each hit leads to a triplet of time-correlated pulses out of the amplifier-discriminator-integrator circuit. The triplet is fed into a time and analogue memory which can store up to 8 hits per wire, then digitized and read into the computer. The correlation between the signals belonging to each triplet is strictly preserved in this process. The electronic circuits and their performance are described in detail in ref. 5. A pulser system allows to inject a pulse of known charge at both ends of each signal wire, in front of each preamplifier. The pulser is used to debug and calibrate the electronic system.

The chamber is contained in an aluminium pressure vessel since it is operated at 4 atm. The pressure vessel allows also to evacuate the chamber volume before filling it with the counting gas, argon - methane - isobutane (0.887:0.085:0.028). At present the chamber is filled with gas, then disconnected from the supply for typically several months. Any influence of atmospheric pressure changes is thereby eliminated. In order to homogenize the gas temperature and composition inside the tank, the gas is continuously pumped around from one side of the chamber to the other via an external bypass. The gas temperature is kept constant to 0.5 degrees.

A solenoid provides a magnetic field of typically 4.5 kG parallel to the axis of the chamber, homogenous to better than 1% over the sensitive volume of the chamber. The magnetic field is orthogonal to the electric drift field and causes therefore a rotation of the drift trajectories by a Lorentz angle approximately 18.5 degrees.

3. Resolutions

3.1. Space resolution: (R,Φ)-plane

The coordinates in the (R,Φ)-plane are determined from the wire position, the measured drift time and the Lorentz angle.

The error on the coordinates contains contributions from errors in the time measurement and in the transformation of time into length as well as from the time spread by electron diffusion along the drift direction. The major contribution to the resolution is the time measurement error, since one TDC time bin is 7.5 ns wide, limited by the maximum clock frequency of the random access memory.

After removal of the effect of the wire staggering, the following corrections are applied to the observed timing, keeping in mind that 1 ns corresponds to 50 μm driftlength:

1) A time slewing correction as function of the signal amplitude and drift time, which on the average is 5 ns.
2) Adjustment of the individual time offset, t_o, for each wire. This value is derived from calibration runs with the pulser system.
3) Correction for time-of-flight of the particles (< 3 ns).
4) Signal propagation time along the anode wire (< 5 ns).

For the transformation of the corrected drift time into a distance ℓ from the anode wire a detailed knowledge is required of the drift trajectories and electric fields in the chamber cells. Fig. 5 shows the trajectories together with lines of equal drift-times. This figure is the result of a computer simulation of one cell, using the measured dependencies of the drift velocity $v_D = v_D(E)$ and of the Lorentz angle $\alpha = \alpha(E)$ [6]. From the drift trajectories a timing correction ΔT is derived which measures the time difference between the first electrons arriving at the wire and the electrons coming from the center of the drift-space. ΔT depends on the drift time t and the angle of the track with respect to the wire plane. The spread in arrival time is biggest for tracks close to the wire plane.

In addition to the computer simulation extensive measurements of the field have been made on an electrostatic model[7], which is more suitable to represent the effect of the strip-shaped field electrodes. The electric field in each cell is uniform over most of the chamber

volume ($\Delta E/E < 2\%$), with bigger deviations near the cell boundaries and the central wire plane. Special timing corrections have to be applied in these regions (3-4 ns).

The measurements on the electrostatic model were also used to determine the relation between the applied voltages and the drift field strength. It is obviously of great importance to choose the drift field such that the dependance of the drift velocity v_D on E is minimal. For 4 atm of the argon - methane - isobutane mixture the best value lies around 940 V/cm, where the drift velocity reaches its maximum v_D = 5.04 cm/µs (Fig. 6). A field inhomogenuity $\Delta E/E=5\%$ gives here $\Delta v_D/v_D$ = 0.15%. A linear space - time correlation is presently used in the analysis after applying the corrections mentioned above.

The space resolution in the (R,Φ)-plane as function of the driftpath ℓ is expected to be of the form[8]

$$\sigma(R,\Phi) = \sqrt{\sigma_{El}^2 + A^2 + B\cdot\ell} \qquad (1)$$

The electronic contribution σ_{El} is 110 µm. The second term, A, is a gas dependant contribution to the resolution at $\ell = 0$ and is discussed in ref. 8. For a gas similar to the one used here A has been measured to be 55 microns. The term $B\cdot\ell$ describes the deterioration of the resolution with increasing drift length due to the electron diffusion.

Fig. 7 shows the measured resolution $\sigma(R,\Phi)$ of a track fit through one cell, averaged over all track angles, as a function of drift length ℓ. The line is a fit according to Equ. (1), with parameters A and B, leaving out the first point since the resolution near the wire is dominated by cluster-fluctuations. The resolution at $\ell = 0$ is 140 µm, to be compared with 125 µm expected from the numbers given above. The origin of the difference is still under study. The degradation of $\sigma(R,\Phi)$ with increasing ℓ is not very important even at a drift length of 5 cm. This is due to statistical effects enhanced by the high gas pressure and the fact that the coefficient for longitudinal diffusion D_L is

smaller than the coefficient for transverse diffusion D_T [8]. The values for D_L and D_T have recently been measured [6] and are shown in Fig. 8.

In Fig. 9 the resolution averaged over all drift distances is shown for cells of ring 1 and 3 which have similar geometric dimensions. The mean value is 155 µm. Also shown is the resolution in ring 2 which is slightly worse due to the greater size of the drift region. The mean resolution in this case is 165 µm. Fig. 10 shows the corresponding distribution resulting from a full track fit through 3 rings. The mean rms deviation, 180 µm, is slightly worse than the single cell values indicating the presence of some systematic errors. A possible source of such errors is the determination of the drift velocity v_D. While the track resolution in a single cell is independent of the precise value v_D, this quantity has to be exactly known for track fits through all 48 points of the chamber. An error of $2^o/oo$ in v_D leads to a systematic shift of the space points of 100 µm for a track passing in 5 cm distance from the wire plane.

3.2. Space resolution: (R,Z)-plane

The coordinate along each wire, Z, is determined by the charge division method. The resolution one can obtain is given by the signal to noise ratio at the preamplifier. From pulser calibration runs one would expect a resolution $\sigma(Z)$ in the order of 1.5 cm corresponding to a signal charge of 0.4 pC. Fig. 11 shows the distribution of rms-deviations from track fits in the (R,Z)-plane. The mean rms is 1.6 cm corresponding to $\Delta L/L$ of 0.6%, where L is the wire lenght, in good agreement with the expectation. The resolution, however, is degraded when several tracks pass through the same detector cell. In this case the individual hits influence each other depending on their amplitude and time separation. The resulting amplitude correlations have to be corrected for. The effect is discussed in section 3.5.

A very important feature for the track fitting in the (R,Z)-plane is the fact that one measures space points rather than projections. Fig. 12a illustrates this point. It shows the (R,Z)-view of a jet event, all tracks being rotated into the same plane. A fit to the different tracks in this projection is quite impossible, however, making use of the (R,ϕ)-view one knows to which track each point belongs and can fit (or display) them individually (Fig. 12b).

3.3. Momentum resolution

The momentum resolution at momenta below 2 GeV/c is mainly determined by multiple scattering. The material inside the jet chamber corresponds to 0.018 radiation lengths from the gas and 0.019 radiation lengths from the two support bars between the three rings. The resulting $\Delta p/p$ is 4 %, with an effective radial track length of 60 cm and B = 4.5 kG. For momenta above 2 GeV/c the resolution obtained at present is $\Delta p/p^2 = 3.3$ % $(\mathrm{GeV/c})^{-1}$.

3.4. dE/dx evaluation

The energy loss in the chamber is calculated from the sum of the pulseheights measured at both ends of the wire. Up to 48 ionisation samplings are measured per track but for jet-like events the mean number of useful samplings is bigger than 30 for only 50 % of all tracks. The reduced sample size comes from tracks which leave the chamber before going through all 3 rings and also from overlapping tracks. To obtain a reliable estimate for the mean energy loss, independent of large Landau fluctuations, the 60 % lowest pulseheights for a given track are averaged and used for particle identification (method of truncated means).

Before averaging, each individual sampling has to be corrected for several effects:

1) The gas- and electronics amplification differs from wire to wire due to slight differences in cell geometry and electronics (integration time, pulseshape etc.). These individual gain-constants have been determined from the electronic pulser and from cosmic ray tracks accumulated during the actual data taking at PETRA. The average of 80 tracks passing a given wire was calculated and plotted versus time. The long-term drift was found to be smaller than 2%.

2) It was found that the pulseheight drops with increasing drift-time due to a contamination of the gas: The effect was negligible right after a new gasfilling and saturated after one month at a 50 % pulseheight drop for the maximum drift time of 1 µs. Therefore each pulseheight was divided by $\exp(-a \cdot t_{drift})$ where a was dependent on the time after the gasfilling.

3) The ionisation is proportional to the sample thickness which is 1 cm for tracks normal to the drift direction. All other tracks have a path length longer than 1 cm and are corrected according to their measured direction.

4) Since the chamber is operated at a gas gain of $4 \cdot 10^4$ an appreciable saturation effect occurs for tracks normal to the wire and for low drift times. The amount of saturation was determined empirically from clean tracks during normal datataking. The corrections are shown in Fig. 13 as function of the drifttime and sin θ, where θ is the angle between track and wire. The slope at short drifttimes has to do with the drift time dispersion. For big drifttimes we observe almost no saturation effect in sin θ whereas for short drifttimes the effect is as big as 25 %. The shape in Fig. 13 depends also on the gasamplification of each individual wire and on the angle γ between track and drift direction.

5) A 6 % negative crosstalk between neighbouring wires was corrected for. This had no influence on the obtained resolution.

3.5. dE/dx resolution

For electrons from Bhabha scattering a resolution of 14 % FWHM is obtained (Fig. 14). These events were selected to have at least 42 samplings per track. Due to the angular distribution of Bhabha events, the effective sample thickness was 1.5 cm on the average and from the investigations of Allison and Cobb[10] one expects for pure argon a resolution of (9-10) %. The discrepancy is not understood at the moment. One possible reason is that the corrections 2) - 4) are not known well enough. Since they amount up to factors of two they have to be known with great precision. If the first and last 100 ns of drifttimes are cut out the resolution improves to 13 % FWHM.

For tracks in jet-like events a degradation in resolution is observed which comes from crossing and overlapping tracks yielding fewer useful samplings per track. Furthermore, the pedestals and electronic gainfactors of successive hits on a given wire are different and only the first hit has been calibrated up to now. In addition, each hit produces a shift in the electronic pedestal due to a slight differentiation of the signal in the preamplifier. This shift is in the order of -10 % of the signal amplitude, decreasing with time. The amplitude of the subsequent hit has to be corrected for this effect. This correction is presently not yet applied.

The observed width for pions in the momentum range of 400 - 500 MeV/c is 24 % FWHM for tracks with at least 25 hits (Fig. 15). Since the mean pulseheight is lower than for electrons a degradation from 14 % to 16 % FWHM is expected[10], everything else being equal. This has been confirmed with muons from cosmic rays. The reduced number of samplings from a mean number of 46 for the electrons to 35 for the pions reduces this resolution to 20 % FWHM. The rest of the discrepancy is attributed to the above mentioned effect of multiple hits.

The difference of the peak position of the pions and electrons

in Fig. 15 gives a relativistic rise of (48 ± 5) % in good agreement with previous measurements [11]. In Fig. 16, a scatterplot, energy loss versus momentum, for particles from beam-gas reactions is shown. Contributions from pions, protons and electrons are visible.

4. Performance

The stability of the complex recording electronics is monitored by the pulser system which also provides the calibration constants for the electronic gain. The stability of the charge measurement including preamplifier, amplifier, integrator, analogue storage and ADC over a period of 9 months is for the majority of the 1536 wires in the order of (1-2) %. After weeding out initial bugs the entire electronic system has proven very reliable.

The integral currents drawn by the 16 anode wires of each cell are constantly monitored during operation. During normal machine running this current is smaller than 2 μA even for the innermost ring. An excessive current in any cell leads to a fast shut down of the high voltage.

A few problems related with the chamber itself have occured during the past operation. In 2 of 96 cells a high voltage breakdown at the feedthrough of the driftfield voltage into the cell has occured. Two cells had to be disconnected when after a two month shutdown and a new gasfilling a glowdischarge formed in these cells.

The measurement of space coordinates and energy loss in the same detector requires a certain number of compromises: to achieve high space resolution a large gas gain is necessary which leads to a small time slewing corrections and a good signal-to-noise ratio, improving thereby the (R,Φ) - and Z-resolution. On the other hand the resolution on dE/dx depends on the amount of corrections which have to be applied to the observed amplitudes.

These corrections become smaller and the resolution better when one decreases the gas gain.

Another compromise affects the double track resolution. The time intervall for charge integration can be varied by the width of a one-shot (Fig.4.).A good double track resolution requires a short integration time while a long integration time improves the dE/dx resolution. The value presently used, 120 ns, has been chosen in order to avoid non-correctable losses in the charge measurement. Because of the priority of data taking under constant instrumental conditions, no variation of this adjustment was tried.

5. Conclusion

The jet chamber of the JADE detector is the first large imaging drift chamber to become operative in an experiment. The design goals were well met and a good long term performance achieved. The values presently obtained for space resolution and dE/dx resolution are near to the expected values, although for particle identification in the region of the relativistic rise the dE/dx resolution needs further improvement. A number of physics results from the JADE detector have already been published [1) 12)].

Acknowledgement

We greatfully acknowledge the contributions of S. Bethke, K.H. Hellenbrand and B. Schmidt who helped us through measurements and discussions to understand better the performance of the detector. We would like to thank the Heidelberg institute workshops for their untiring efforts in the construction of the detector and the read-out electronics and for their competent help during the installation of the chamber at PETRA.

References

1) W. Bartel et al., JADE Collaboration, Phys.Lett. 88B, 171 (1979)

2) J. Heintze, Nucl. Instr. and Meth. 156, 227 (1978)
W. Farr et al., Nucl. Instr. and Meth. 156, 283 (1978)
H. Drumm et al., IEEE Trans Nucl. Sci. 26.1, 81 (1979)

3) D. Schmidt, Proceedings of the Wire Chamber Conference, Vienna 1980, to be published in Nucl. Instr. and Meth.
M.Atac, ibid.

4) See second part of this report

5) W. Farr and J. Heintze, Nucl. Instr. and Meth. 156, 301 (1978)

6) B. Schmitt, Diplomarbeit, Phys.Inst. der Univ. Heidelberg (1980) and private communication.

7) S. Bethke, Diplomarbeit, Phys.Inst. der Univ. Heidelberg (1980) private communication.

8) W. Farr et al., Nucl. Inst. and Meth. 154, 175 (1978)

9) J.J. Lowke and J.H. Parker, Phys.Rev. 181, 302 (1969)

10) W.W.M. Allison and J.H. Cobb, Univ. of Oxford, Preprint 13/80

11) A.H. Walenta et al., Nucl. Inst. and Meth. 161, 45 (1979)

12) W. Bartel et al., JADE Collaboration, Phys.Lett. 89B, 136 (1979), DESY 79/77, DESY 79/80, DESY 80/04, DESY 80/14.

Figure Captions

1) The JADE detector.

2) Cross-section through two segments of the jet-chamber. ℓ is the length of the drift path, α the Lorentz angle.

3) Picture of a typical jet-event. x : hits assigned to tracks by pattern recognition. ı: unassigned hits.

4) Schematic diagram of the jet-chamber electronics.

5) Drift trajectories and lines of equal drift times (dashed curves)

6) Drift velocity v_D as a function of the electrical field E (argon-methane-isobutane 0.887 : 0.085 : 0.028 atm)

7) Mean rms deviation of single cell track fits in the (R, ϕ)-plane as function of the mean drift distance. The arrows indicate the cell dimensions in ring 1-3 resp. Further details see text.

8) Coefficients for longitudinal and transversal diffusion D_L and D_T as function of the reduced fieldstrength E/p. μ is the electron mobility. Data from Ref. 6. The curves are eye-fits assuming dependencies similar to those obtained for pure argon[9].

9) Single cell track fits, (R,ϕ)-plane: distribution of rms deviations. Full line: Ring 1 and 3; dashed line: Ring 2.

10) Track fits through 3 rings, (R,ϕ)-plane: distribution of rms deviations.

11) Single cell track fits, (R,Z)-plane: distribution of rms deviations.

12) Jet-event projected onto (R,Z)-plane. (a) All tracks shown. (b) Same event, two tracks selected, using information from (R,ϕ)-reconstruction.

13) Relative pulseheight per unit track length as function of sin θ and drift time.

14) Landau distribution and truncated mean for electrons from Bhabha scattering.

15) dE/dx distribution for particles from jet like events (momentum range 400-500 MeV/c, mostly pions). The distribution for electrons from Bhabha events is also shown.

16) Energy loss as function of momentum. Particles from beam-gas reactions E_{beam} = 15 GeV.

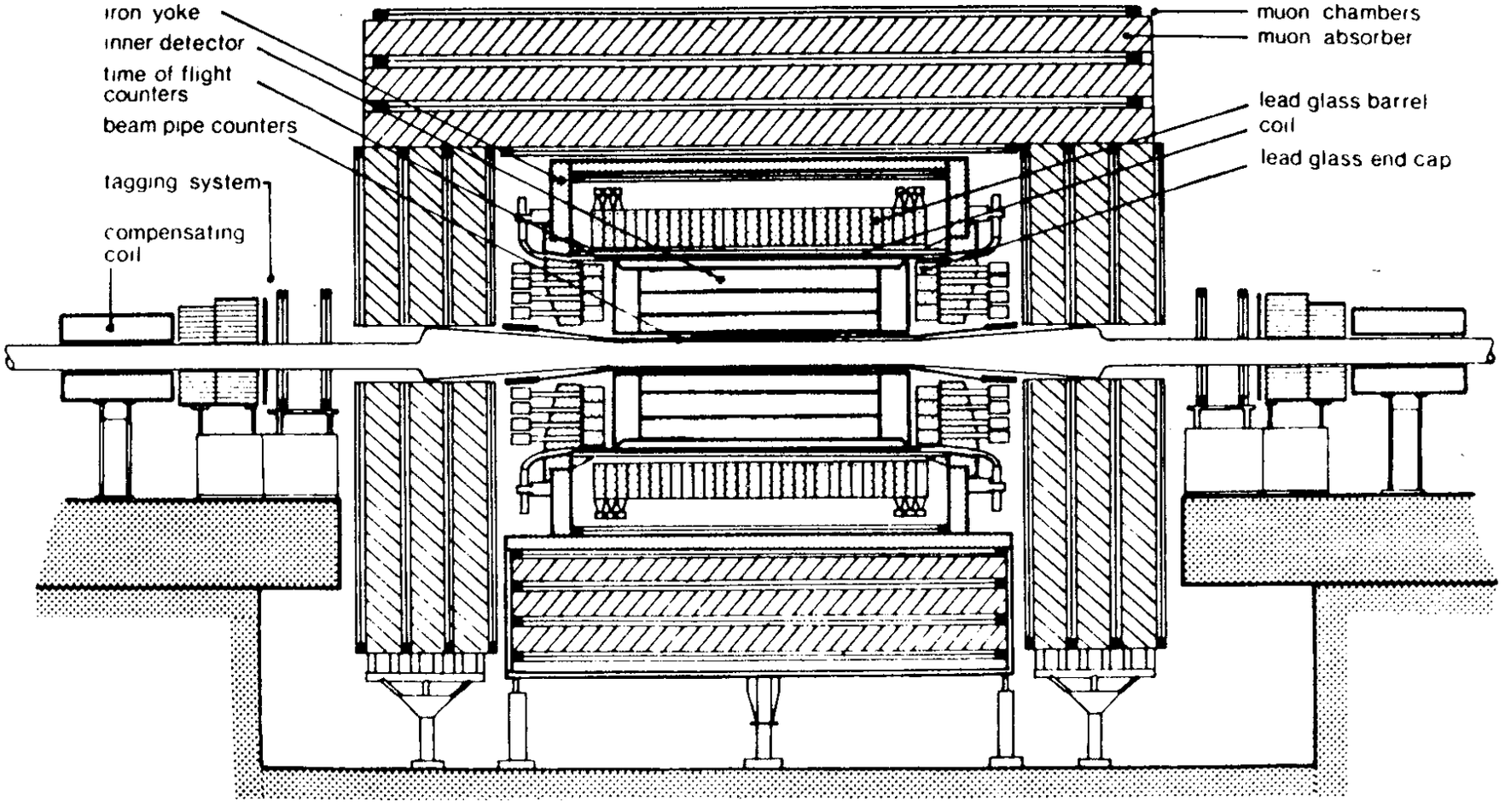
iron yoke
inner detector
time of flight counters
beam pipe counters
tagging system
compensating coil
muon chambers
muon absorber
lead glass barrel
coil
lead glass end cap

Fig.1

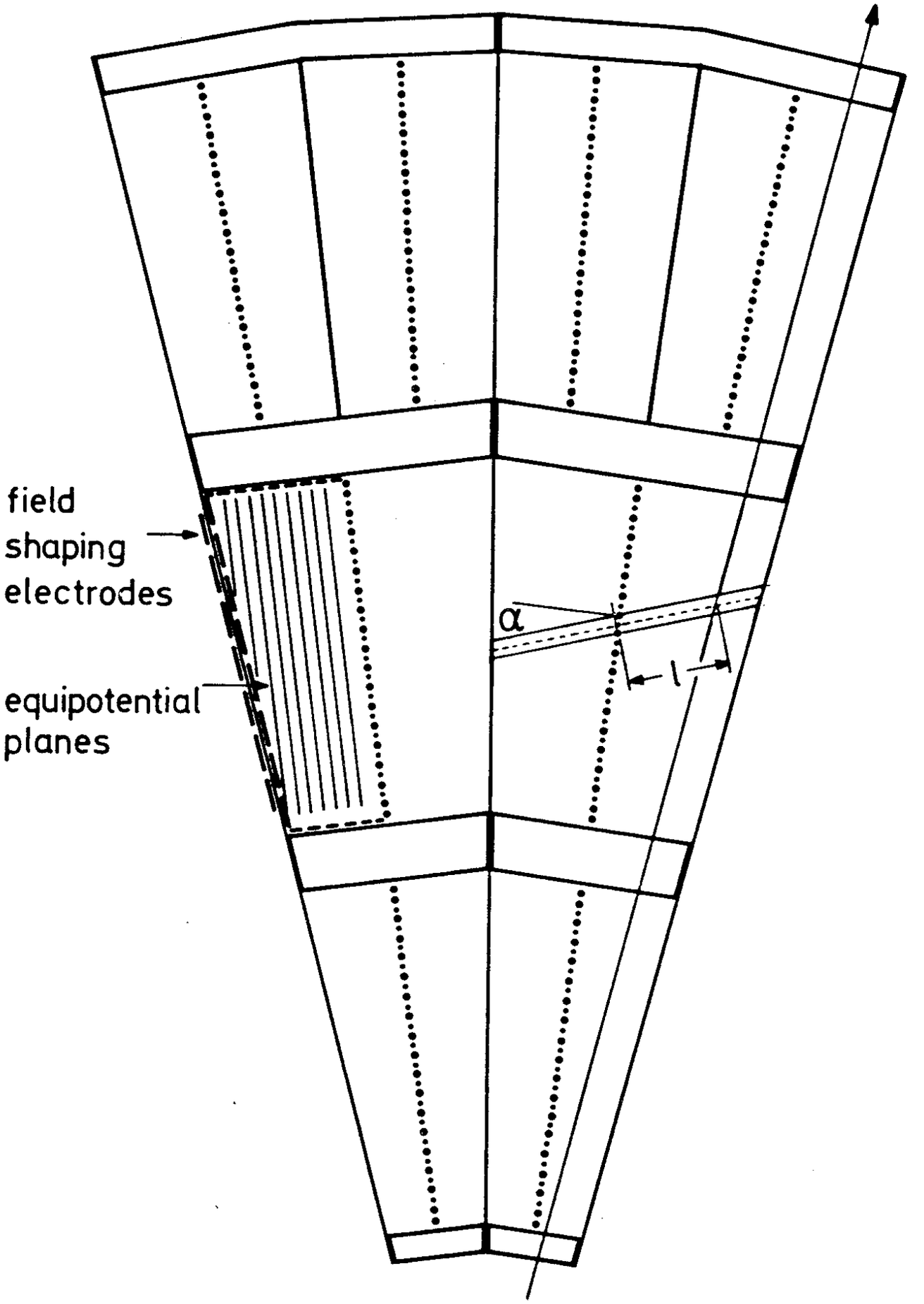

Fig. 2

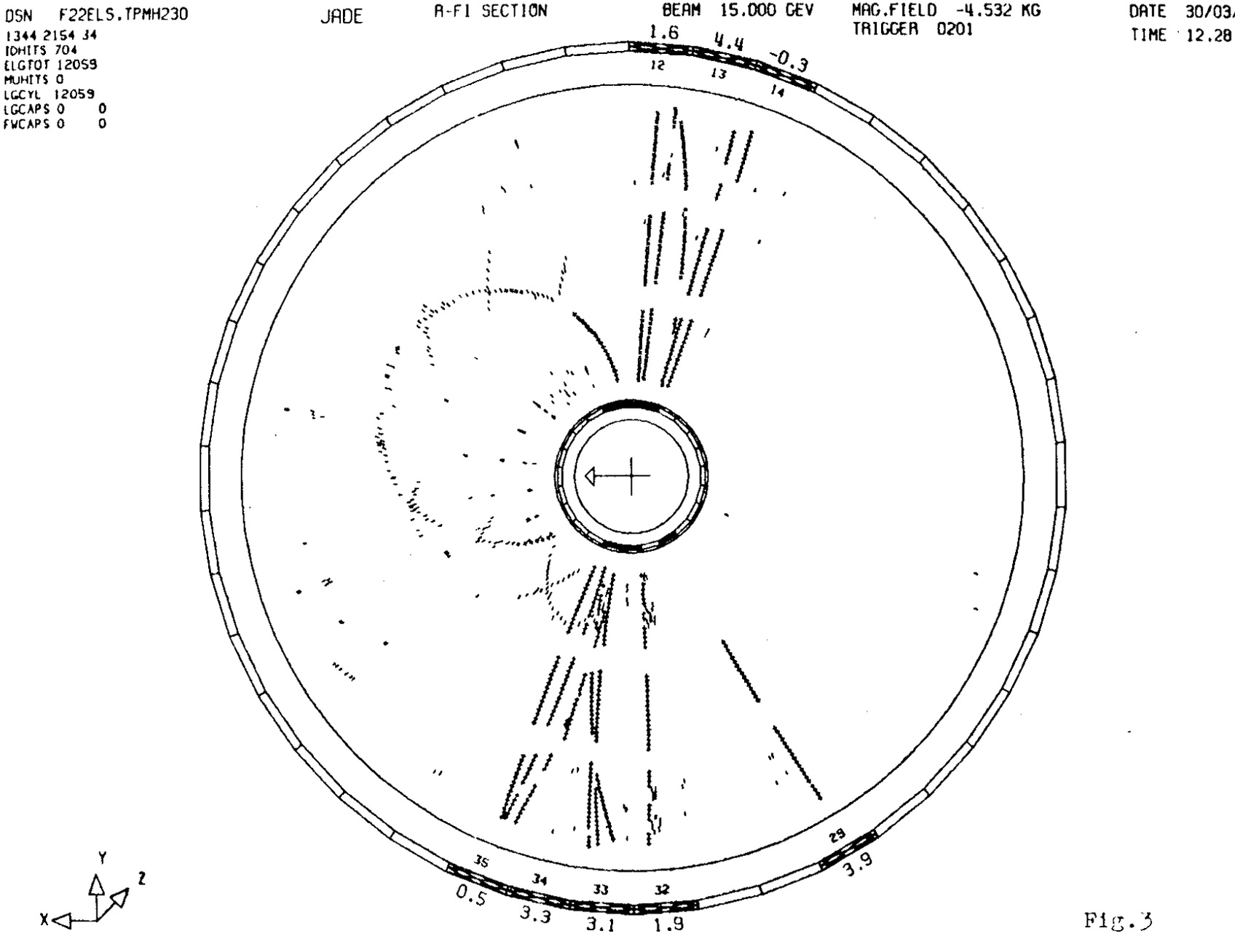
DSN F22ELS.TPMH230
1344 2154 34
IDHITS 704
ELGTOT 12059
MUHITS 0
LGCYL 12059
LGCAPS 0 0
FWCAPS 0 0
JADE
R-FI SECTION
BEAM 15.000 GEV
MAG.FIELD -4.532 KG
TRIGGER 0201
DATE 30/03/80
TIME 12.28.16
1.6
4.4
-0.3
12
13
14
29
3.9
35
34
33
32
0.5
3.3
3.1
1.9
Y
Z
X

Fig.3

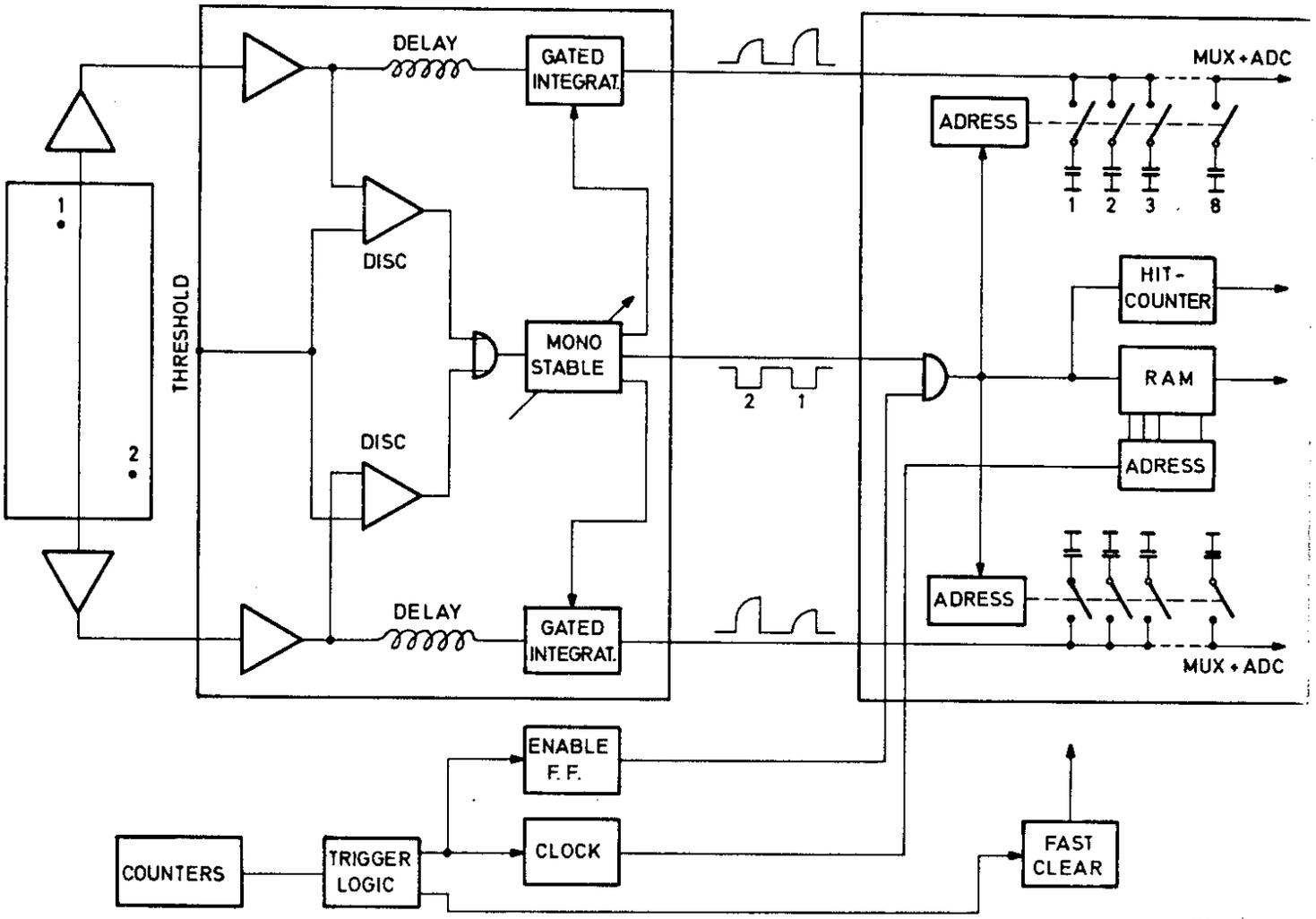
DELAY
GATED INTEGRAT.
MUX + ADC
ADRESS
1
2
3
8
1
2
THRESHOLD
DISC
MONO STABLE
HIT-COUNTER
RAM
2 1
DISC
ADRESS
ADRESS
DELAY
GATED INTEGRAT.
MUX + ADC
ENABLE F.F.
COUNTERS
TRIGGER LOGIC
CLOCK
FAST CLEAR

Fig.4

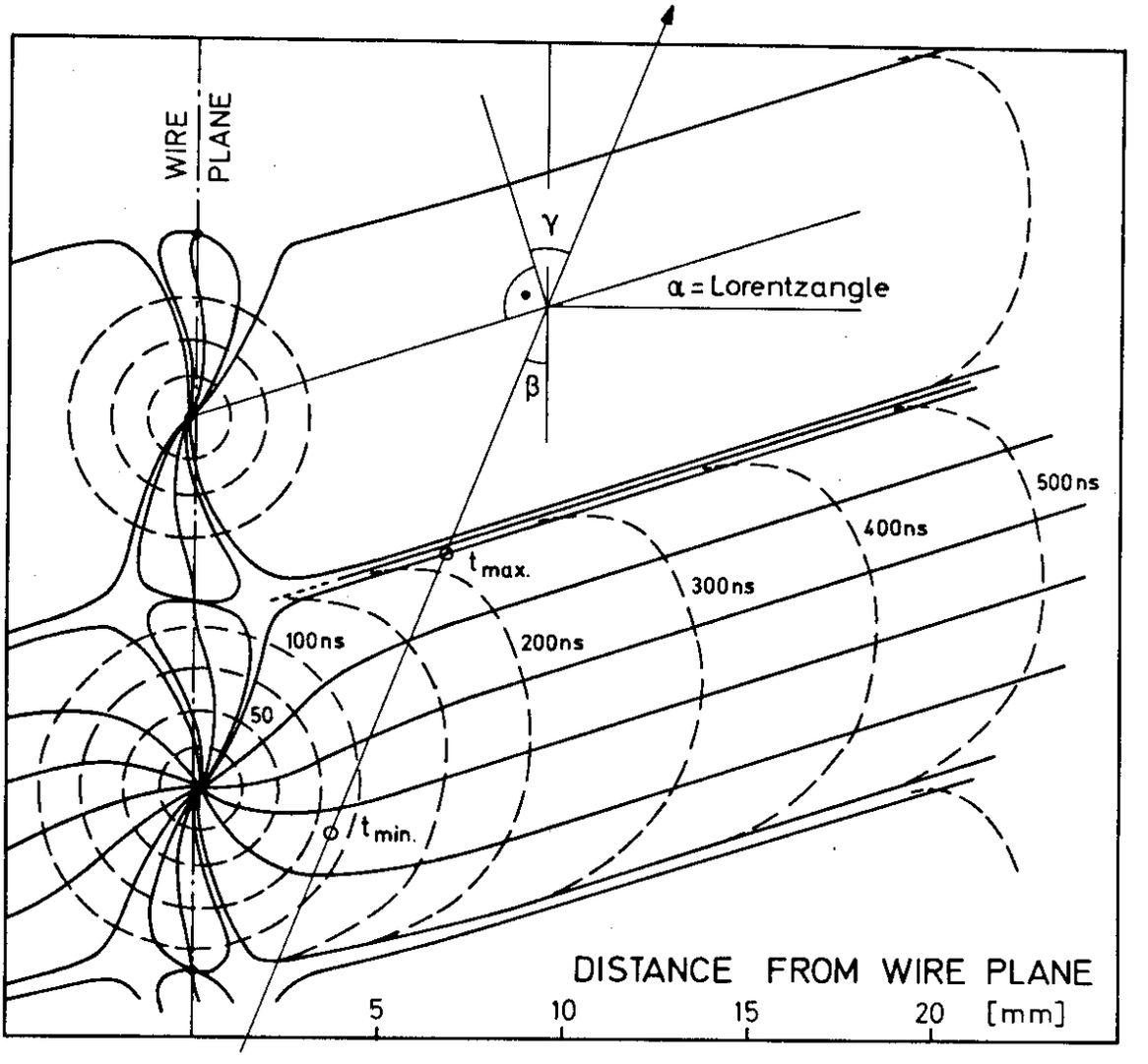
WIRE PLANE
γ
α = Lorentzangle
β
500ns
400ns
300ns
200ns
100ns
50
$t_{max.}$
$t_{min.}$
DISTANCE FROM WIRE PLANE
5
10
15
20
[mm]

Fig.5

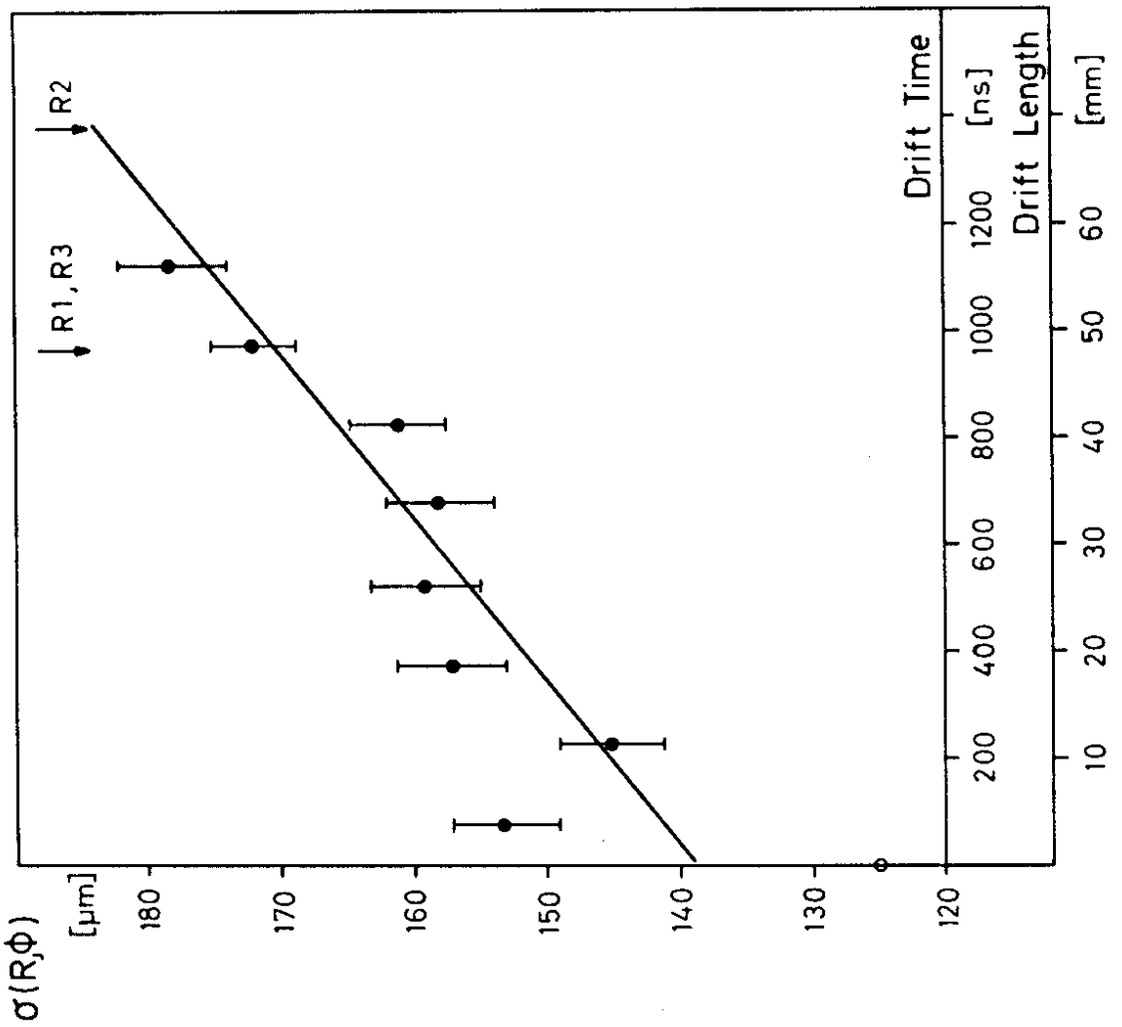
R2
R1, R3
Drift Time [ns]
Drift Length [mm]
σ(R,Φ) [μm]
180
170
160
150
140
130
120
200
400
600
800
1000
1200
10
20
30
40
50
60

Fig. 7

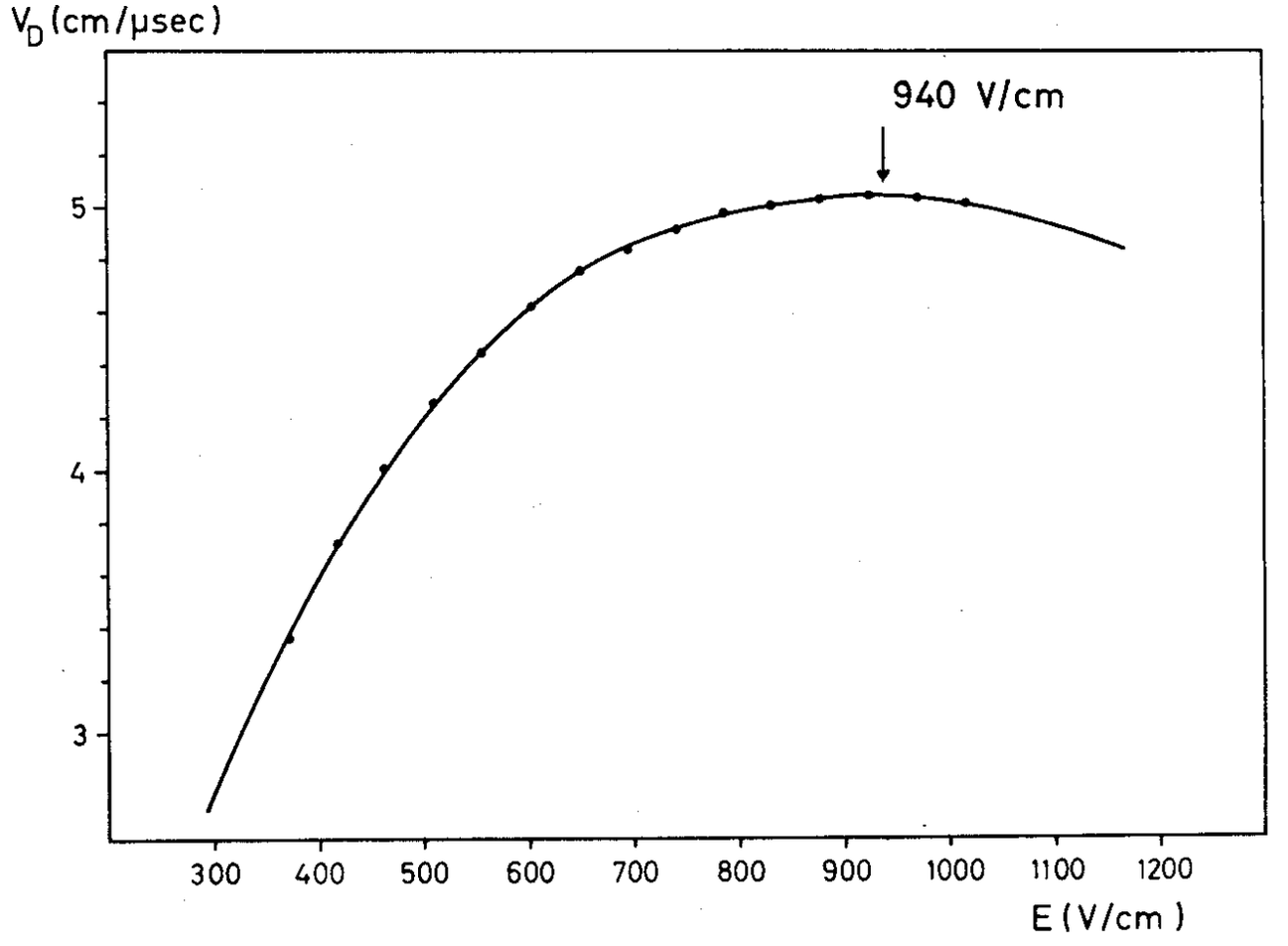
V_D (cm/μsec)
940 V/cm
5
4
3
300
400
500
600
700
800
900
1000
1100
1200
E (V/cm)

Fig.6

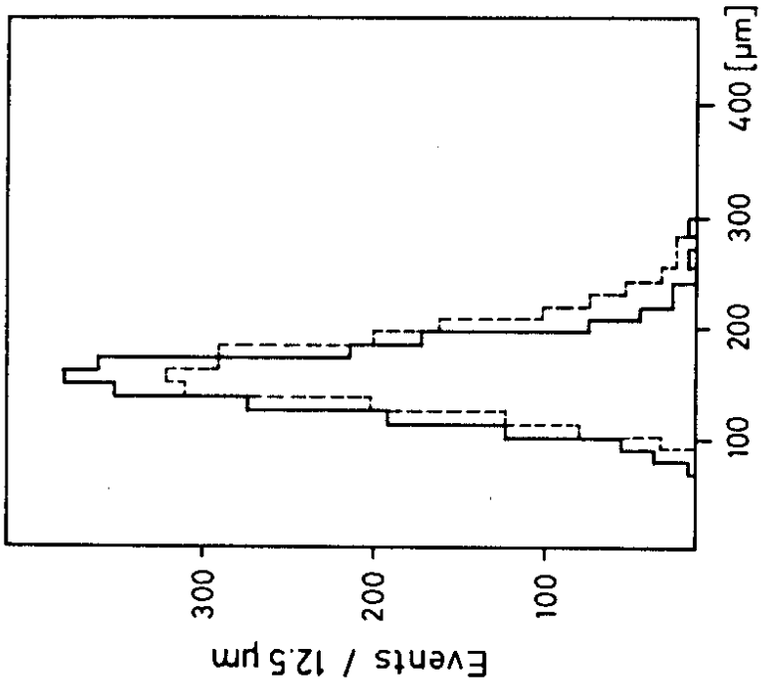
Events / 12.5 μm
300
200
100
σ (R,Φ)
100
200
300
400 [μm]

Fig.9

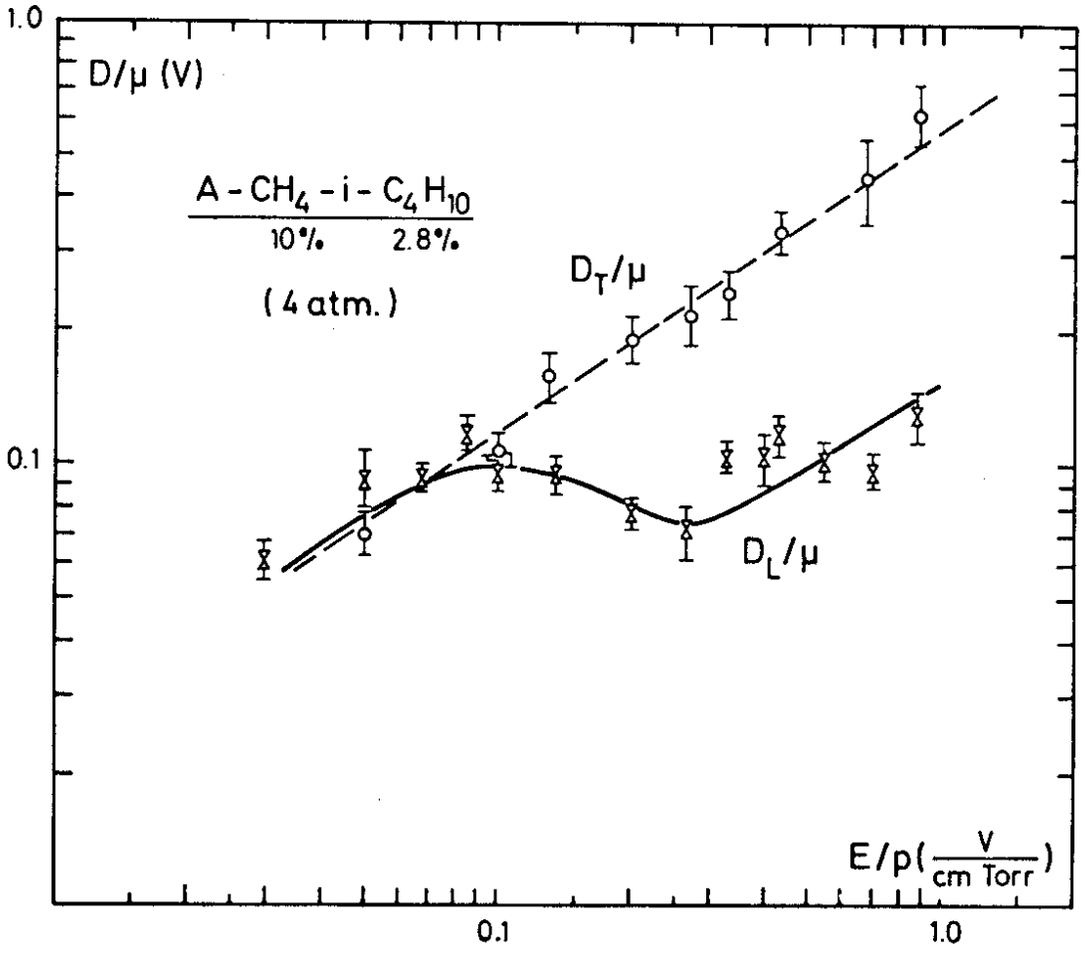
D/μ (V)
1.0
0.1
A - CH4 - i - C4 H10
10% 2.8%
(4 atm.)
DT/μ
DL/μ
E/p(V / cm Torr)
0.1
1.0

Fig.8

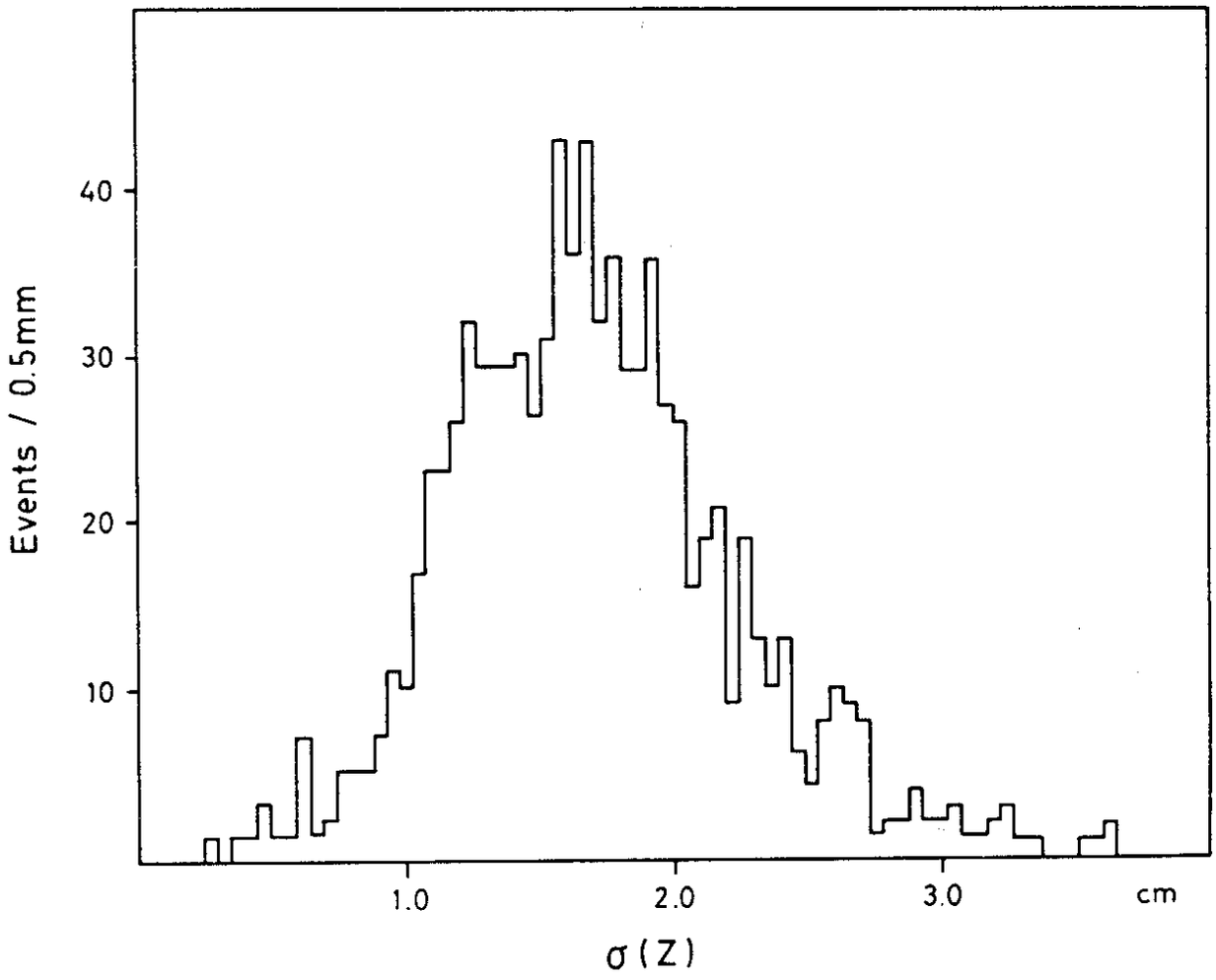
Events / 0.5mm
40
30
20
10
1.0
2.0
3.0
cm
σ (Z)

Fig. 11

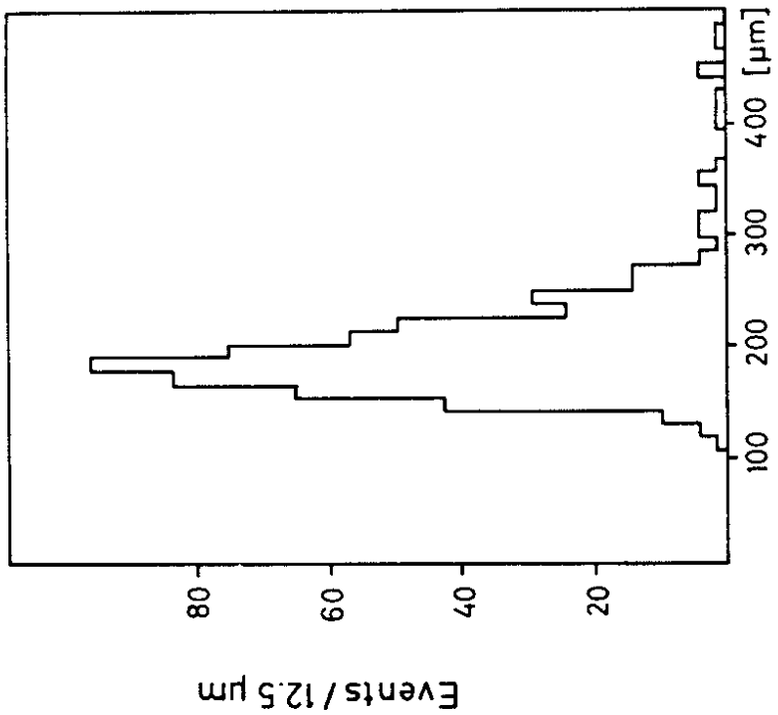
Events / 12.5 μm
80
60
40
20
σ (R,φ)
100
200
300
400 [μm]

Fig. 10

PLOT STARTED AT 115116 ON [illegible]
PLOT RECEIVED FROM FI1WAG TSUSER NEWLIBT MODULE JADE ON SYSTEM C

DSN FI10L5.MUMAC27.NEWCAL JADE Z-X SECTION BEAM 13.866 GEV MAG.FIELD -4.537 KG DATE 17/08/79
1099 2674 157 TRIGGER 0201 TIME 11.35.53
IDHITS 696 NR OF TRACKS 17 NR OF TR.ELEMENTS 61
ELGTOT 14538
MUHITS 0
LGCYL 14518
LGCAPS 0 0
FWHITS

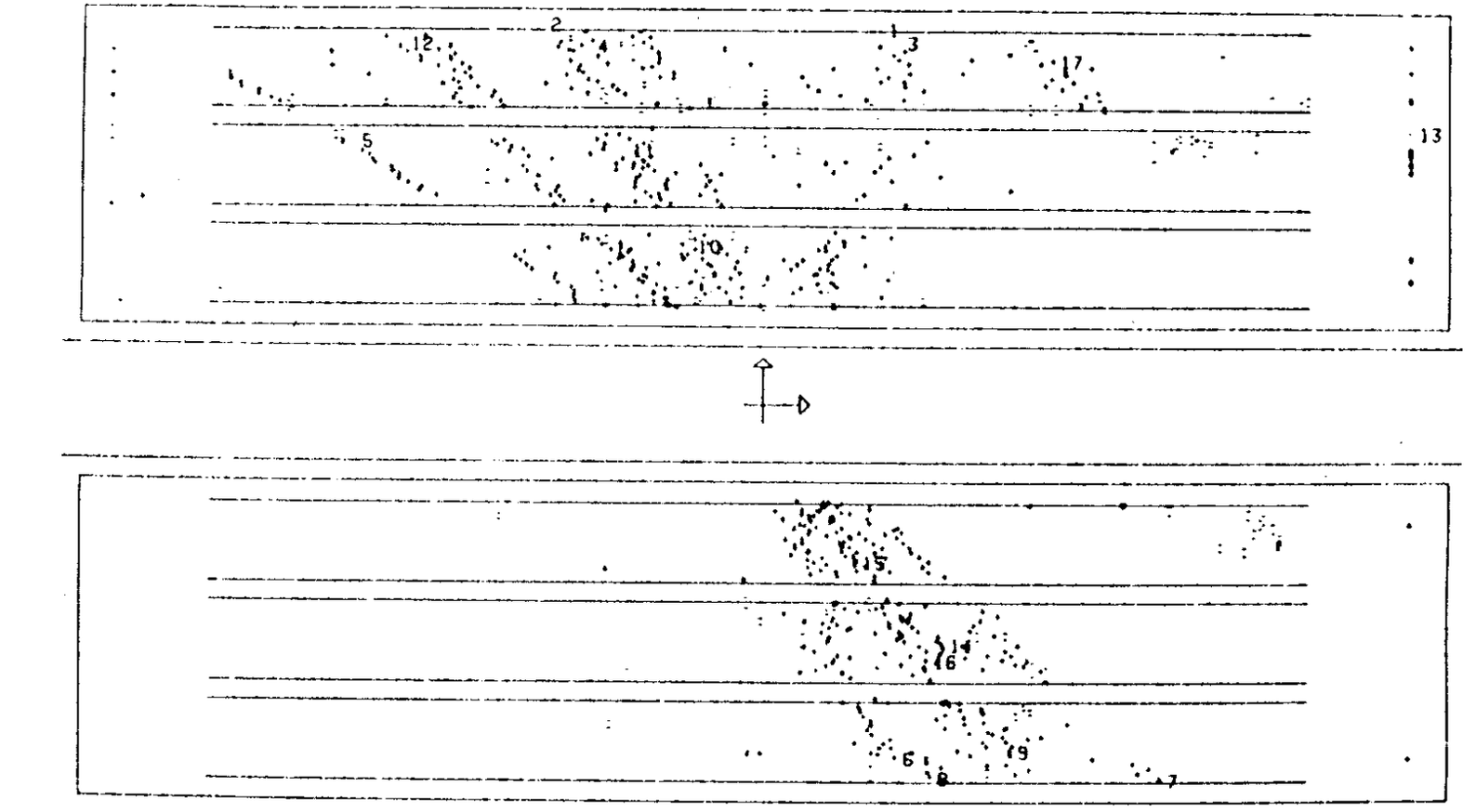

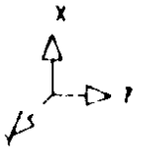

Fig.12a

DSN F110LS.MUHAD27.NEWCAL JADE Z-X SECTION BEAM 13.866 GF MAG.FIELD -4.537 KG DATE 17/08/79
TRIGGER 0201 TIME 11.31.31
NR OF TRACKS 17 NR OF TR.ELEMENTS 61

1099 2674 157
IDHITS 696
ELGTOT 14638
MUHITS 0
LGCYL 14638
LGCAPS 0 0
FWHITS

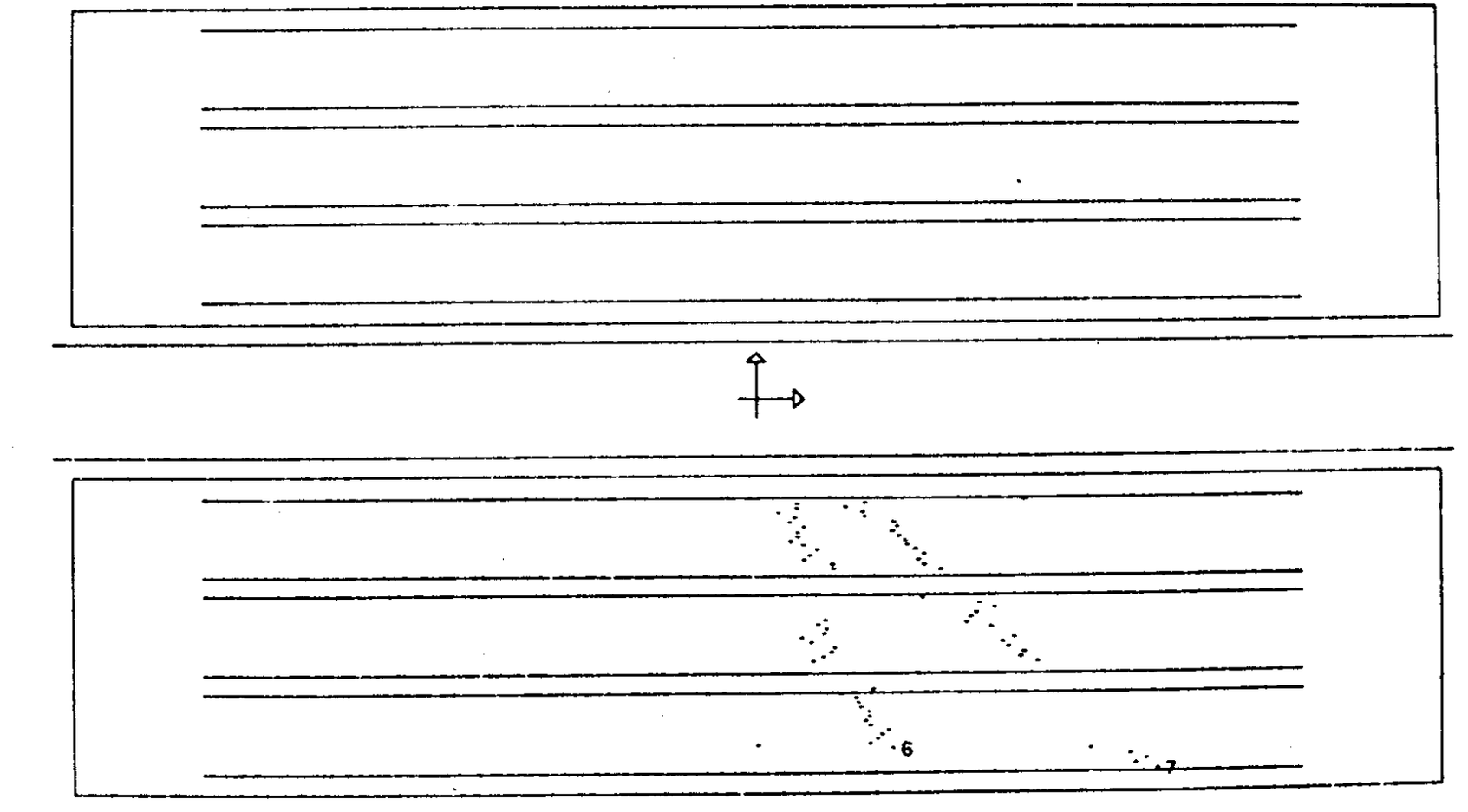

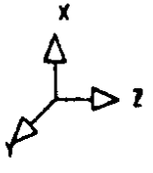

Fig.12b

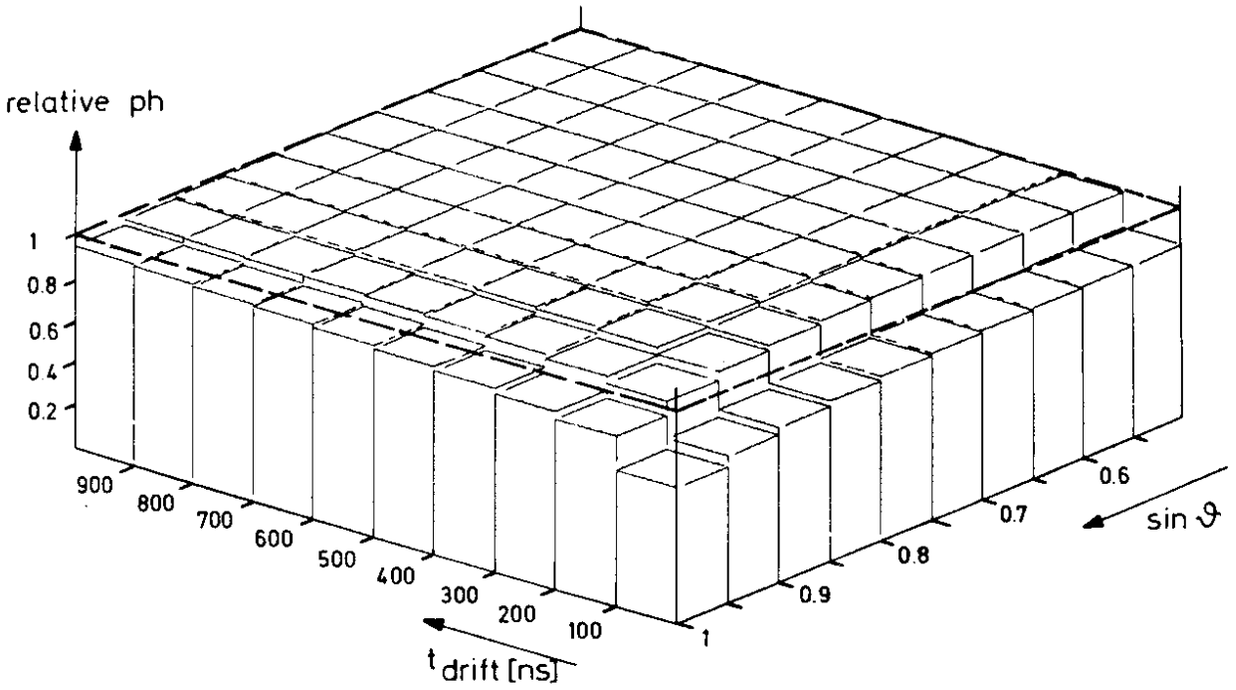
relative ph
1
0.8
0.6
0.4
0.2
900
800
700
600
500
400
300
200
100
t drift [ns]
1
0.9
0.8
0.7
0.6
sin ϑ

Fig. 13

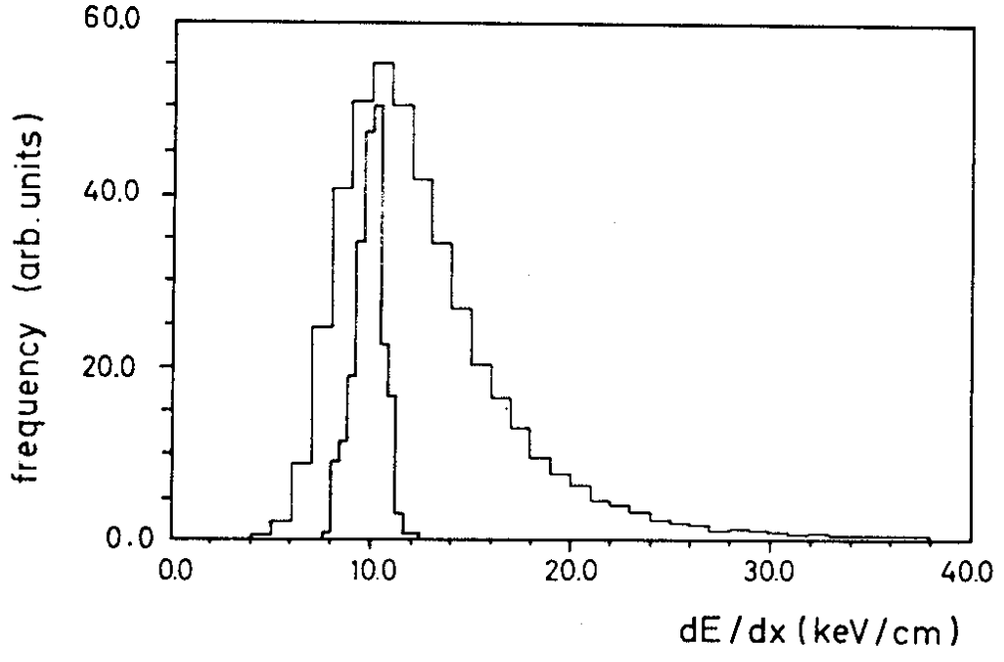
60.0
40.0
20.0
0.0
frequency (arb. units)
0.0
10.0
20.0
30.0
40.0
dE / dx (keV / cm)

Fig. 14

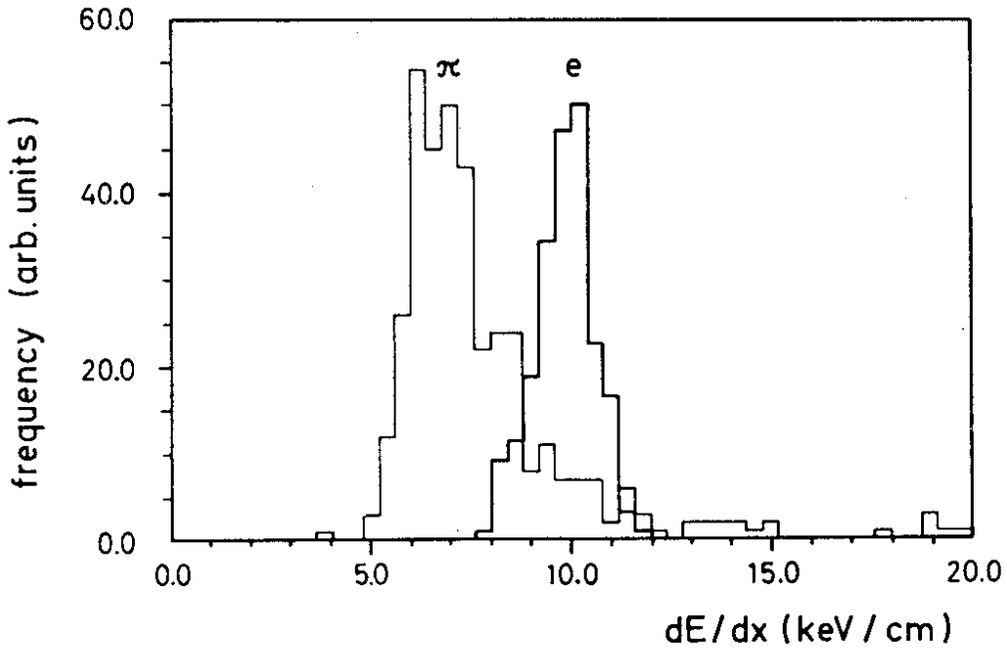
60.0
40.0
20.0
0.0
frequency (arb. units)
π
e
0.0
5.0
10.0
15.0
20.0
dE/dx (keV/cm)

Fig. 15

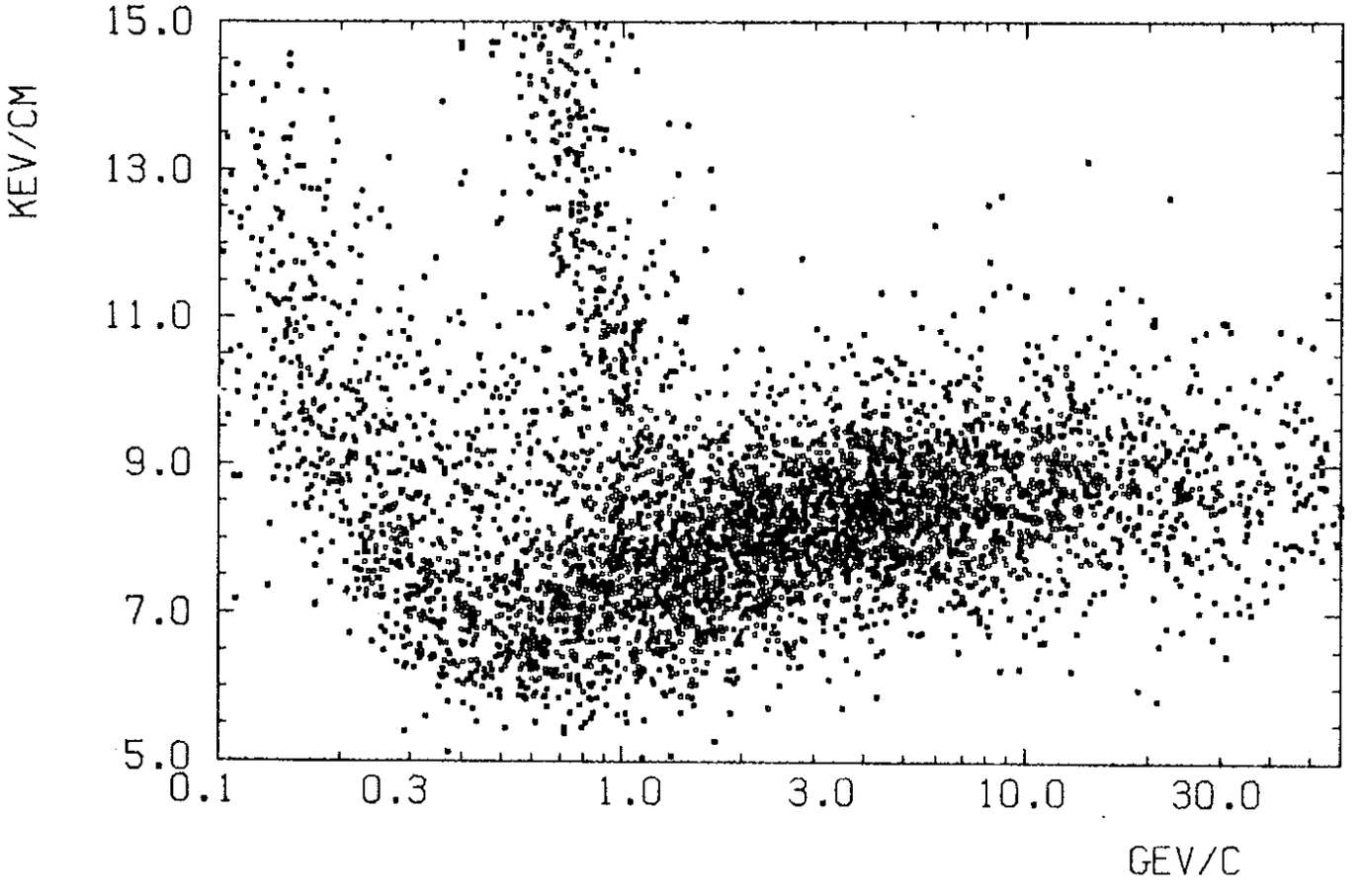

Fig.16

Part 2 :

1. Introduction

An important part of the JADE detector (ref. 1) are the central jet chambers which provide up to 48 independent measurements for each charged track detected. In order to convert these measurements into momentum and dE/dX, which can be used in a physics analysis of the events, a comprehensive pattern-recognition program is required. In this paper we describe the development and present status of such a program.

The paper is organised in six sections as follows. In section 2 we describe the data input and output formats used and present some relevant features of the jet chambers. In the third section we describe a fast method to determine the event vertex along the beam axis without prior track finding. In section 4 the detailed features of track finding are presented and in section 5 we show how the pattern recognition programs are incorporated into an interactive graphics system. Finally in section 6 the program efficiency and time consumption are given.

2. Detector and input-output data format

We describe here some features of the JADE jet chambers which are important for pattern recognition. A more detailed description of the chambers can be found elsewhere (ref. 2).

The jet chambers consist of three concentric rings of 24, 24 and 48 cells (see fig. 1). The cells are grouped into sectors with one cell from rings 1 and 2 and two cells from ring 3. Each cell contains 16 sense wires parallel to the magnetic field of the detector[+]. The electric field is orthogonal to the wire plane, and the 0.5 Tesla magnetic field causes the drift directions to be inclined by 18.5 degrees with respect to the electric field (see fig. 2). For each track the drift times and the amplitudes (A+,A-) at both ends of the sense wires are recorded. The x and y coordinates of the hit are determined from the wire number and drift time and the z coordinate of the hit is calculated from the two amplitudes using the charge division method,

$$z = \text{const.}\ (A+ - A-)/(A+ + A-).$$

[+] We use a cylindrical coordinate system with the z-axis parallel to the beam axis, the magnetic-field direction and the sense wires.

As indicated in fig. 2, a track passing through a cell in the radial direction in general produces 16 sets of measurements. Therefore, in passing through all three rings, 48 space point measurements of track position are obtained. The multi-hit electronics used allow up to 8 hits to be recorded on a single wire. The drift time alone is not sufficient to determine whether a charged particle passes on the left or the right side of the wire plane. Each track, therefore, has an apparent mirror on the opposite side of the wire plane. However, the sense wires in the jet chambers are staggered by +/- 200 microns in the direction orthogonal to the wire plane, making the drift time measurements on the correct side smooth while the mirror track appears staggered (see fig. 2). This effect is used to solve the left-right ambiguity.

If two tracks have drift distances differing by less than 7 mm (double hit resolution) then no hit is recorded for the track which is farther from the wire plane (see tracks 2 and 3 in Fig. 2), and the z-coordinate determined for the closer track is wrong due to the overlap of the amplitude of both tracks. In addition one observes a distortion of the drifttime and amplitude measurement between 7 and 12 mm (e.g. track 3 in Fig. 2). This effect can be explained by the yet incomplete correction for the second hit on a wire.

All input and output data from the different parts of the JADE detector are organized in a bank structure. The raw jet-chamber data form a bank of 16-bit words. The first part contains pointers to the first hit in each of the 96 cells. Then follow the actual data with four words for each hit, grouped according to cell number:

1) wire number and hit number on this wire
2) amplitude (-)
3) amplitude (+)
4) drift time in units of about 7 nanoseconds (0.4 mm)

The results of the track finding programs are stored in two different output banks. The hit-label bank contains two 16-bit words for each measured hit which encode the correlation between hits and tracks. If a hit has been associated to a track, the track number and left-right assignment are stored in the first word. If it has also been associated to a second track, the second word is filled. In addition each hit label contains information on the fit residuals for this hit and has a bit set if the z measurement is wrong. This bank is used

in the dE/dX mass assignment programs and also allows at a later stage the recalibration of the data or more refined track fitting without having to redo the pattern recognition.

The track bank contains, for each track, information about fit parameters, number of hits, start and end points etc.

3. Z-vertex determination

Events from beam-beam interactions originate from a limited region of about 5 cm along the z-axis. However, background events such as cosmic rays or beam-gas interactions have a flat z-vertex distribution. Therefore a first selection of beam-beam interactions can be made as soon as the z coordinate of the vertex is known. For this purpose a fast program has been developed to determine the z-vertex without prior track finding.

Since the magnetic field is parallel to the z-axis, all tracks with a transverse momentum of more than 100 MeV/c are straight lines in the r-z plane. The method for the fast z-vertex determination uses this fact in the following way:

Any two hits on corresponding wires in ring 1 and ring 2 are selected either in the same or adjacent sectors. The z coordinates are calculated from the amplitudes and the r coordinates are approximated by the wire distances from the origin. The intercept with the z-axis of the line joining the two hits is entered into a histogram. This is repeated throughout the detector for all combinations of two hits. Therefore, for each track in the detector, 16 measurements of its intersection with the z-axis are obtained and a peak is produced in the histogram. Combinations of hits from two different tracks or from hits not on any track will only contribute to a flat background in the histogram. Since the event vertex corresponds to a common point of intersection of all the tracks, it appears as a peak above a flat background. The position of this peak gives the z-vertex. If several peaks are observed (e.g. a cosmic ray in coincidence with a beam-beam interaction) the peak closest to the interaction point is chosen. In this way the z-vertex is found to an accuracy of about 25 mm.

This program is used in a first stage data reduction to reject background events and takes about 1 msec/track on an IBM 370/168 computer. A data-reduction factor of four is obtained if only events with a z-vertex closer than 350 mm from the interaction point are kept.

4. Track finding

The resolution of the drift-time measurement is two orders of magnitude better than the z measurement. For this reason the track finding is done in the x-y plane. The corresponding z-coordinates are obtained automatically, since the chamber measures points in space.

The reconstruction of the tracks in the jet chambers proceeds in three steps:

step 1: search for track elements within a cell.
step 2: assignment of track elements to tracks.
step 3: fit of the tracks and search for additional hits

Step 1

In step 1 track elements are created. These are pieces of a complete track containing four or more hits all of which are in one cell. It is not the intention at this stage to find all hits belonging to a track in a cell, but only a sufficient number to determine values for the position, direction and curvature of the track elements. These parameters are stored for use in the second step.

Track elements are searched for by first creating line elements. These consist of three hits on three successive wires satisfying the conditions:

$$|0.5(D(I+1)+D(I-1)) - D(I)| < 1.5 \text{ mm}$$
$$|D(I)-D(I-1)| < 10 \text{ mm}$$
$$|D(I)-D(I+1)| < 10 \text{ mm}$$

where D(I) is the drift distance of the hit on the I'th wire. Only hits for tracks with transverse momenta of less than 50 MeV/c do not fulfill this condition. Hits which are connected to each other via line elements form a track-element candidate. A parabola in wire number and drift space coordinates is then fitted to the candidate. The deviations of the hits from the fitted curve are calculated for both the left and the right ambiguity, after correcting for the

wire staggering. The better solution is chosen and the candidate is considered a good track element if the average deviation is less than 0.24 mm. If the fit is worse than this and does not improve by rejecting the two worst hits, the track element is assumed to consist of hits from two crossing tracks. It is then cut at the point of biggest slope difference between line elements and both parts are fitted independently. The position, direction, curvature and flag for left-right solution are stored for use in step 2. This procedure is repeated for all cells that contain at least four hits.

Step 2

In the second step the track elements are connected to form tracks. Starting in the outer ring a track element is extrapolated inwards (using its stored parameters) to find an unused element. If the connection is successful the track elements are marked as used, assigned to the track and extrapolated further inwards. For track elements with more than 7 hits, the left-right solution previously determined from wire staggering is used, for shorter track elements both solutions are tried. In this manner a complete track is built up from track elements. The procedure is repeated until all track elements are assigned to tracks.

The decision whether to connect track elements is made in one of two ways, either a fast method or a slower but more efficient method.

In the faster method a connection is made if the drift time and the slope (change of drift time with wire number) agree within preset limits with those expected from the extrapolation. In addition, the connection to this track element must be better than the connection to any nearby track element. For low multiplicity events this method is found to be quite efficient and is used for event selection in our first stage data reduction.

In the slower, more efficient method each connection is checked by a parabola fit to the x-y coordinates of all hits associated with the track elements. This method is used for events that are analysed for physics results.

Step 3

In the third step all hits on the track elements assigned to a track are assembled and their x-y coordinates calculated. A parabola fit (or a circle fit for transverse momenta less than 500 MeV/c) is then made to these hits and the fit parameters used to both interpolate and extrapolate the track in order to collect all remaining hits. Both isolated hits not attached to any track element and entire track elements not previously assigned to the track may be picked up in this way. If more than three additional hits are found by this search, a new fit is made and the whole procedure repeated until the complete track has been found.

The hits correlated with a track in x-y are now used to fit a straight line in the r-z plane. However, since some of the z-measurements of a track may be wrong (see section 2), hits with bad z coordinates must be recognized before a fit can be attempted. The intercept of the track with the z-axis is determined by a histogram method similar to that described in section 3. Using this intercept, the slope for each hit is entered into a new histogram. A peak in this histogram indicates the average slope of the track so that hits outside the peak are rejected. A straight line fit to the hits within the peak is then made.

Finally, the fit parameters from the x-y fits and from the r-z fits are stored in the track bank and the hits correlated with the tracks marked in the hit-label bank.

As an example of this track-finding program, we show in fig. 3 a magnified section of a jet event taken with the JADE detector. Fig. 3a) shows the data before pattern recognition while in fig.3b) only the hits correlated with tracks by the pattern-recognition program are shown.

5. Graphics

The pattern-recognition programs described above have been developed to be used within the JADE graphics display system. The standard display options of magnifying interesting areas or choosing one of several views of the detector are available. Special display commands exist to examine in detail the workings of the pattern recognition. These include the possibility to display track ele-

ments belonging to any track, display non-assigned hits, suppress mirror hits, etc. The pattern recognition can also be paused after step 2 and intermediate results examined or changed. Another useful feature is the ability to change any of the internal program limits at the graphics terminal and to immediately see the effect of the new limits. These options have proved to be of particular value in the development of the pattern recognition programs.

An editing capability has also been developed allowing manual intervention to guide the course of the track-finding program. The editing of an event takes place between steps 2 and 3, (i.e. after the connection of track elements and before the final fits of the tracks). The pattern recognition is halted and the editor can change the result obtained up to this point. In particular the editor can delete or create track elements, reverse the left-right assignment of track elements or tracks, or change the assignment of track elements to tracks. After each change the editor is able to see how the event would look with these modifications. The editing of events using the JADE graphics display has allowed us to obtain correct events for physics analysis in the early stages of program development.

6. Timing and efficiency

On an IBM 370/168 computer the track-finding programs use from 20 to 28 msec./track if the fast method is chosen and from 45 to 115 msec./track for the slower method. The two different times for each method are for low multiplicity events and for high multiplicity jet events.

Inefficiencies in the track finding come from several sources. The jet chambers have a reduced efficiency for detecting tracks passing close to the cell sidewalls and the drift times of the recorded hits are distorted. This may lead to complete tracks not being found if they pass close to the cell sidewalls in all three rings. In fact half of our present inefficiency is due to this. As mentioned in section 2, if tracks are close together the hits having the larger drift time are distorted. This may cause track elements to be wrongly connected and tracks to be only partially found or wrongly extrapolated.

Based on data taken by JADE at PETRA we have estimated our track-finding efficiency. We have considered only tracks originating from the interaction

point (i. e. we have excluded secondaries from beam-pipe scattering and back scatters from the magnet coil) with a momentum greater than 100 MeV/c. For low multiplicity events where all tracks are well separated our efficiency is essentially 100 %. For jet events at a beam energy of about 16 GeV (approximately 18 tracks/event) our efficiency is 97 % to correctly find a track and 75 % for an event to have all tracks correct. This agrees with efficiency studies made on Monte-Carlo generated events.

The track-finding programs are still under development and the efficiency and time consumption are expected to improve.

References

1. W. Bartel et al., JADE collaboration, Phys. Letts. 88B (1979) 171
2. see first part of this report.

Figure captions

1. Schematic drawing of the cell structure of one quadrant of the cylindrical jet-chamber detector. The hatched area shows a sector of the detector.
2. Single cell of the jet-chamber detector. The dots show the sense wires, the crosses the potential wires and the hatched area the drift space of a single sense wire. Three tracks passing through the cell are indicated by dotted lines. The hits produced by the tracks on the sense wires are indicated by long dashes.
3. Magnified area of a jet event at 33 GeV center of mass energy taken with the JADE detector.
   a) All hits with mirrors.
   b) Only hits correlated with tracks by the pattern recognition.

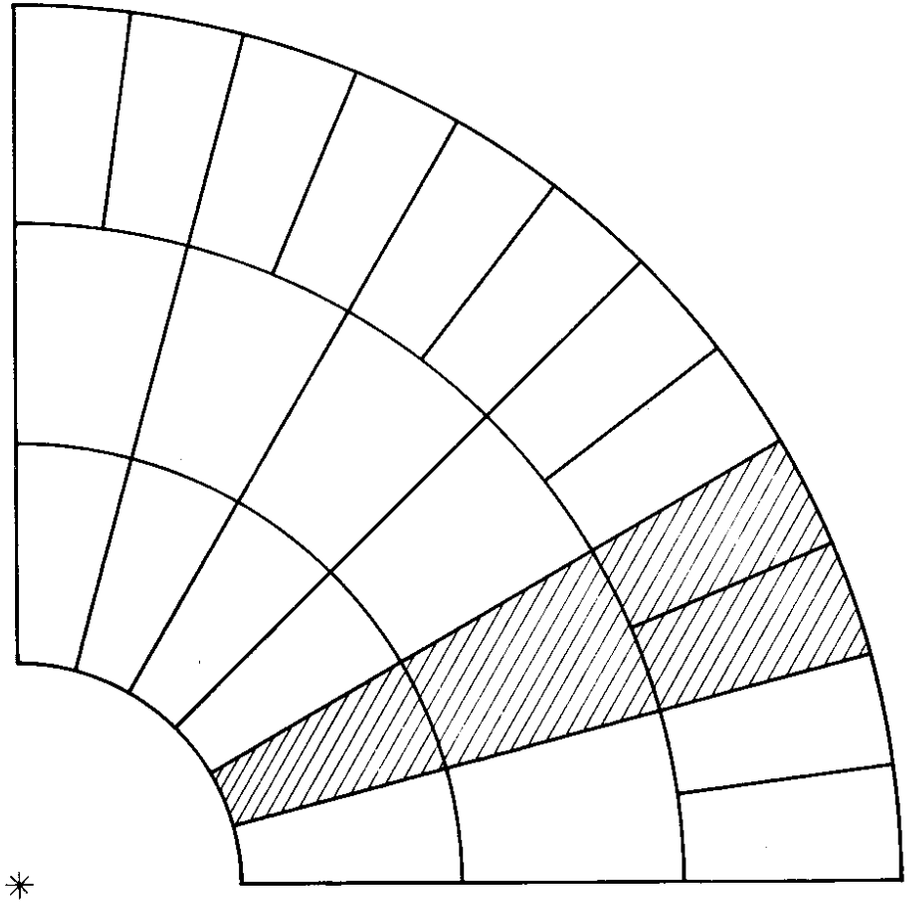

FIG.1

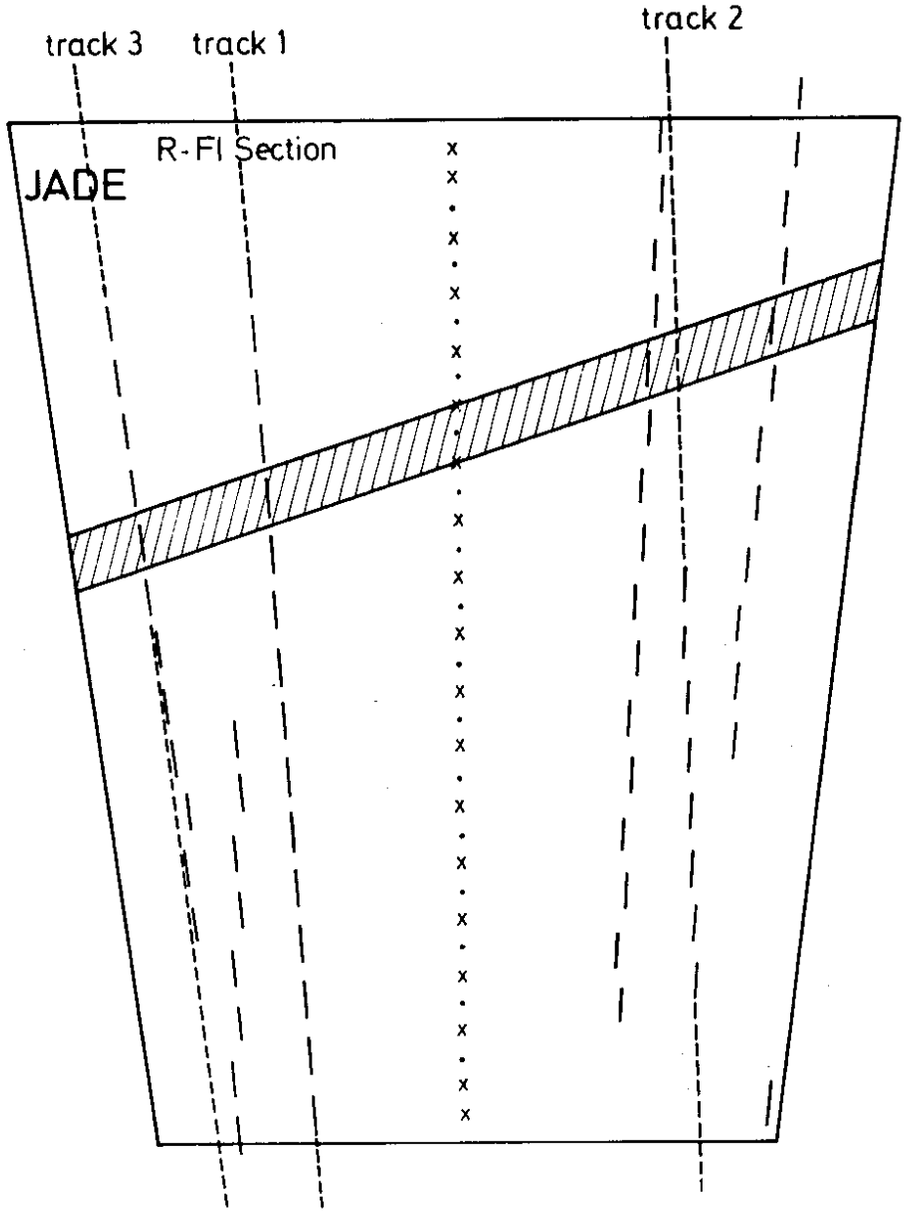

FIG. 2

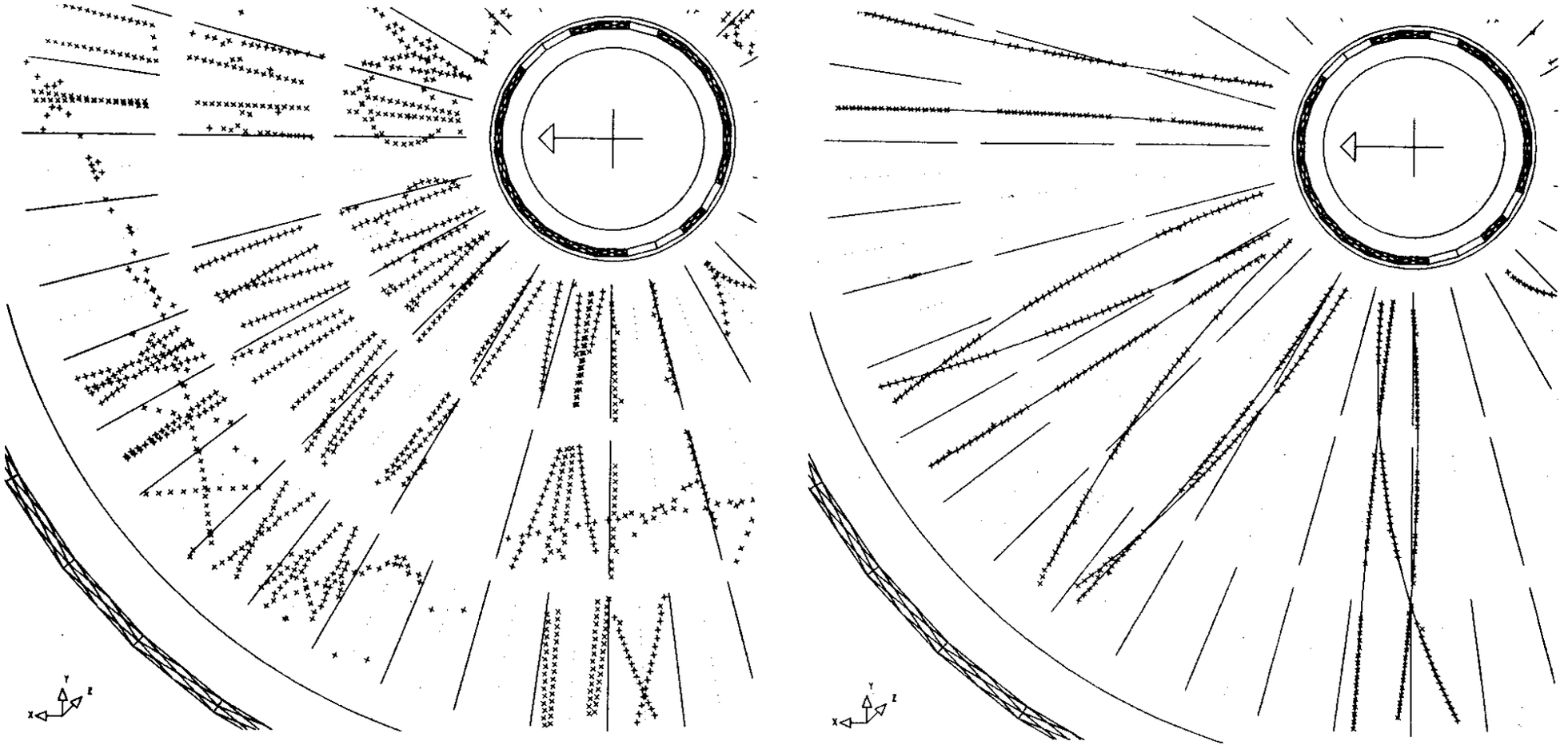

29936

Fig.3